

2.2 CHANGES IN THE EARTH'S RESOLVED OUTGOING LONGWAVE RADIATION FIELD AS SEEN FROM THE IRIS AND IMG INSTRUMENTS

H.E. Brindley*, P.J. Sagoo, R. J. Bantges and J.E. Harries
Imperial College, London, UK

1. INTRODUCTION

Several authors have suggested the possibility of utilizing measurements of spectrally resolved outgoing longwave radiation (OLR) to monitor the climatic state (e.g. Goody et al., 1998). The idea is attractive since even a moderate degree of spectral resolution allows the assignation of changes seen in the OLR to a particular cause. However, its practical implementation has been hampered by a lack of suitable observational data.

Two data sets which have become available for analysis are provided by the Infrared Interferometer Spectrometer (IRIS), and the Interferometric Monitor for Greenhouse Gases (IMG). IRIS flew on the Nimbus 4 satellite, taking observations from April 1970 to January 1971 (Hanel et al., 1972). IMG, flying on the ADEOS satellite, produced a set of similar measurements spanning October 1996 to June 1997 (Kobayashi et al., 1999). A comparison of the data was reported by Harries et al (2001), and indicated that clear signatures of increases in greenhouse gases between the two measurement periods could be identified in the OLR difference spectrum.

Because of the length of the observational records used, the study by Harries et al. was limited to a comparison between two distinct periods in time. Given the variability within the climate system, a valid question to be addressed is the degree to which high frequency events may have influenced the magnitude of the signal reported. One obvious candidate that would be expected to exert a large influence on the temperature and water vapour fields at any given point in time is the El Nino Southern Oscillation (ENSO). Since the classic response of the climate system is seen within the equatorial Pacific we confine our attention to this region. By using model simulations of the resolved OLR over two extended time intervals centred on each measurement period the impact of short-term variability is assessed. In all cases, the

simulations and data presented here correspond to clear-sky conditions only.

2. DATA CHARACTERISTICS AND PROCESSING

2.1 The IRIS Instrument

The IRIS-D Michelson interferometer provided measurements of the radiance leaving the top of the Earth's atmosphere over the spectral range 400 to 1600 cm^{-1} with a nominal apodized resolution of 2.8 cm^{-1} . The Sun-synchronous nature of the satellite orbit resulted in two global sweeps per day, with nominal equator crossing times of noon and midnight. The instrument had a circular field of view of approximate diameter 100 km. Every fifteenth and sixteenth interferogram was taken whilst viewing a warm blackbody and cold outer space respectively to achieve calibration. For one spectrum, the noise equivalent radiance is quoted as varying from 0.5 to 1.0 $\text{mW m}^{-2} (\text{cm}^{-1})^{-1} \text{sr}^{-1}$ from band centre to edge.

2.2 The IMG Instrument

A Michelson interferometer type instrument, IMG was designed to allow the retrieval of detailed greenhouse gas profiles from OLR measurements made in 3 spectral bands. For the purposes of this study band 3 data, running from 600 to 2000 cm^{-1} , was employed. The spectral resolution within this band increases from 0.25 cm^{-1} (at 1800 cm^{-1}) to 0.1 cm^{-1} (at 700 cm^{-1}) due to the alignment of the band 3 detector. Placed in a Sun-synchronous, 41-day recurrent polar orbit at 800 km, IMG had a field of view of 64 km^2 . Radiometric calibration was achieved using observations of an internal warm blackbody and deep space after every six Earth views. For an individual spectrum, this is believed to provide a relative uncertainty of 0.20 - 0.27 $\text{mW m}^{-2} (\text{cm}^{-1})^{-1} \text{sr}^{-1}$.

2.3 Quality control and cloud-clearing

Before accepting any of the spectra measured by either instrument strict quality control was performed on both sets of data. As a first step, spectra that had been classified as unreliable by the given science team were removed. The IMG data was then smoothed to match the

* *Corresponding author address:* Helen E. Brindley, Space and Atmospheric Physics Group, Imperial College, London, SW7 2BZ, UK; e-mail: h.brindley@ic.ac.uk

IRIS spectral resolution, and a small multiplicative correction was applied to the wavenumber scale to account for the effects of the different solid angles subtended at the two instruments. Radiances were then converted to equivalent brightness temperatures (BT).

Calculations on the remaining IMG data showed unacceptably high BT standard deviations at the centre of the 667 cm^{-1} CO_2 band and so it was decided to set the lower wavenumber limit for both instruments at 710 cm^{-1} . Similarly, the upper wavenumber was set at 1400 cm^{-1} since the noise in the IRIS data substantially increased at wavenumbers greater than this value.

Clear sky spectra were then derived for both instruments using a two-step brightness temperature threshold technique. The first step compared the BT at a wavenumber where the atmosphere is at its most transparent (1127.7 cm^{-1}) with the underlying sea surface temperature taken from NCEP reanalyses. If the magnitude of the difference in temperature was greater than a set threshold then the spectra was rejected as cloudy. Thresholds were selected by finding the value above which the standard deviation of the remaining spectra remained approximately constant across the window region ($850\text{-}1250\text{ cm}^{-1}$). Although this initial step should remove all but the warmest optically thick clouds, a second test was employed in an attempt to remove the effects of absorption due to thin cirrus. Following the example of Ackerman et al. (1990), this test compared the BT at 901.1 cm^{-1} ($\sim 11\text{ }\mu\text{m}$) and 1197.2 cm^{-1} ($\sim 8\text{ }\mu\text{m}$). Because of the absorption characteristics of ice it would be expected that if cirrus were present the BT difference ($8\text{ }\mu\text{m}\text{-}11\text{ }\mu\text{m}$: $\text{BT}_{(8-11)}$) should be greater than in the corresponding clear-sky situation. Given this, for each geographical region investigated, an optimum $\text{BT}_{(8-11)}$ was empirically selected. If the $\text{BT}_{(8-11)}$ for an individual spectrum exceeded this threshold the spectrum was rejected as cloudy. The thresholds were chosen based on the twin requirements to minimize the standard deviation across the window of the 'clear' spectra, whilst retaining enough spectra to form a statistically significant average. Sensitivity studies have indicated that the basic shapes of the final clear-sky difference spectra are relatively insensitive to the exact thresholds selected.

3. SIMULATION METHODOLOGY

Pentad mean global temperatures and specific humidity fields representative of two twenty-seven month intervals centred on the operational periods of the two instruments, running from April 1969 to June 1971, and April 1996 to June 1998 were generated using the Hadley

Centre Atmospheric Model version 3 (HADAM3). HADAM3 comprises the atmospheric portion of the Hadley Centre Coupled Climate Model, with 19 levels in the vertical, and a horizontal resolution of 2.5° latitude x 3.75° longitude.

The model was forced by observed sea surface temperatures taken from the Global Sea Ice and Sea Surface Temperature (GISST) data set, and also included the effects of changes in trace gases, and a parameterisation of volcanic and solar forcing over the period considered. In order to quantify the impact of model uncertainties, four realizations of the atmospheric state were provided.

Using the model geophysical fields along with representative values of trace gas concentrations for each period, radiance spectra were calculated for each grid point and month at 1 cm^{-1} resolution over the wavenumber range $600\text{-}1400\text{ cm}^{-1}$ by the MODTRAN3.7 radiative transfer code. These 1 cm^{-1} radiances were then degraded to 2.8 cm^{-1} resolution using the IRIS instrument function and converted to the equivalent BT.

4. SAMPLING CHARACTERISTICS

The amount of noise on the radiance spectra presented here is reduced via temporal and spatial averaging of the individual spectra recorded by each instrument. Temporally, in an effort to remove the effects of seasonality from the results, only spectra from the months April, May and June (AMJ) in 1970 and 1997 are used to form the IRIS and IMG averages respectively. Nevertheless, the temporal distribution of the clear-sky spectra do show distinct differences between the two instruments in certain regions with, in general, IMG tending to provide more measurements in April relative to May and June, whilst IRIS observations are more uniformly scattered over the three months. This may in itself be an interesting consequence of changes in cloud pattern between the observational periods but obviously presents difficulties when attempting to compare a perfectly sampled model field with the data. By focusing on the equatorial Pacific, where the inter-monthly atmospheric variability should be at a minimum, we circumvent this problem. The two geographical regions considered span a latitude range of 10° S to 10° N , with longitudinal extent $160\text{-}215^\circ\text{ E}$ (West Pacific) and $215\text{-}270^\circ\text{ E}$ (East Pacific). Table 1 provides information concerning the number of samples used for each area and time.

TABLE 1. Number Of Clear-sky Spectra Used To Create Space/time Averages For IMG/IRIS

Spatial Region	IRIS	IMG
West Pacific	118	50
East Pacific	63	111

5. RESULTS

The observed 1997-1970 AMJ change in BT for the west Pacific and east Pacific regions are shown in figure 1. Also indicated on each plot is the envelope of maximum uncertainty associated with the difference plot, calculated by assuming that the quoted error on each spectrum is systematic in nature. The shape of the difference curves is remarkably consistent across both regions with spectral features due to CO₂ (710-740 cm⁻¹, 800 cm⁻¹), CFC11 (840-850 cm⁻¹), CFC12 (900-920 cm⁻¹), O₃ (1000-1070 cm⁻¹) and CH₄ (1280-1310 cm⁻¹) clearly apparent. Both curves also show enhanced emission over the atmospheric window with a clear break at the O₃ band. Differences shortwave of the band are consistently lower than those on the longwave side. Such a signature could be attributed to residual thin cloud in the nominally clear spectra. Given this, inferences concerning changes in surface temperature should be made with caution. Nonetheless, the larger increase in window BT over the east Pacific compared to that seen in the west is consistent with the phase of ENSO over the two measurement periods.

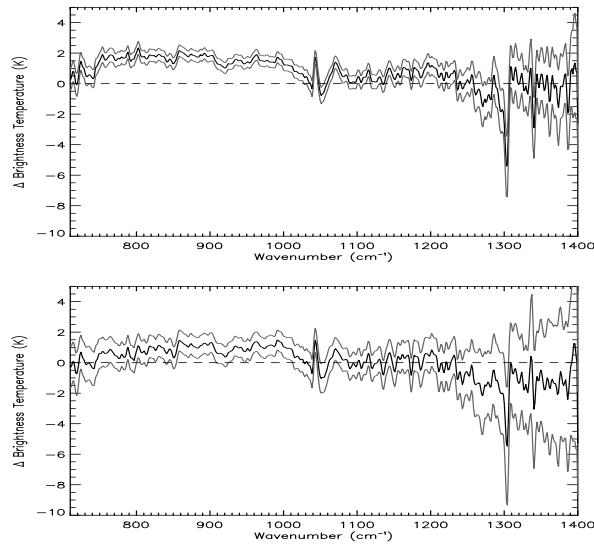


Figure 1. IMG-IRIS change in AMJ mean brightness temperature with associated uncertainty range. Top: East Pacific; Bottom: West Pacific

Figure 2 illustrates the changes between the 1970 and 1997 AMJ mean atmospheric temperature and humidity profiles generated by HADAM3. The crosses at each level highlight the 1- σ spread in these mean values over the 4 realisations considered. In both regions warming and moistening is predicted at all tropospheric levels. This moistening is sufficient to increase the level relative humidities by up to 10 %. In the stratosphere a strong ozone induced cooling is seen.

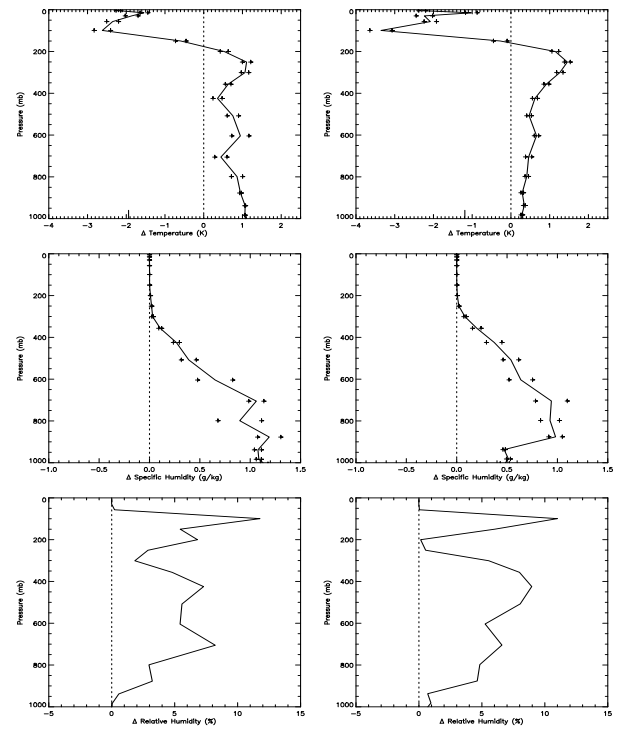


Figure 2. 1997-1970 AMJ mean changes in temperature and humidity derived from HADAM3. Left: East Pacific; Right: West Pacific

Simulated BT change spectra are presented in figures 3 and 4 for the east and west Pacific respectively. To investigate the relative role of the temperature and humidity changes the upper plot in both cases indicates the effect of only changing individual components on the BT difference, with the combined effect over-plotted in bold. For both regions the enhanced water vapour fields tend to dominate the BT response, strongly modulating the enhanced emission due to surface and tropospheric temperature increases in both shape and magnitude. Clearly however, considering changes in humidity and temperature alone cannot explain the shape of the observed BT difference spectra (fig. 1).

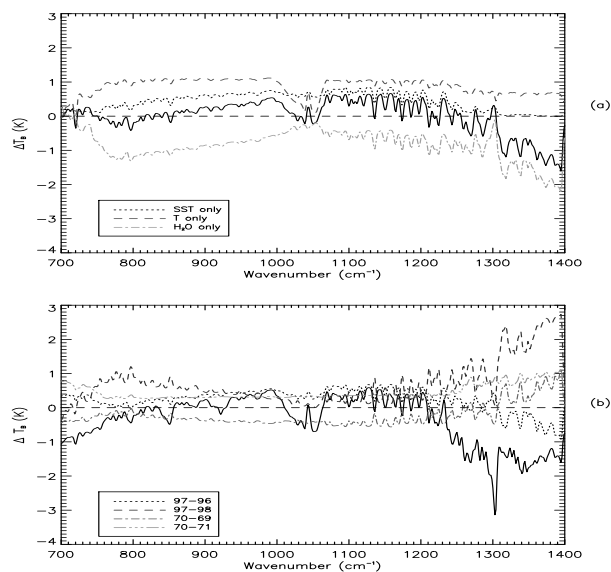


Figure 3. East Pacific: (a) Influence of SST, temperature and humidity on the simulated AMJ 97-70 difference; (b) Inter-annual variability in difference signal.

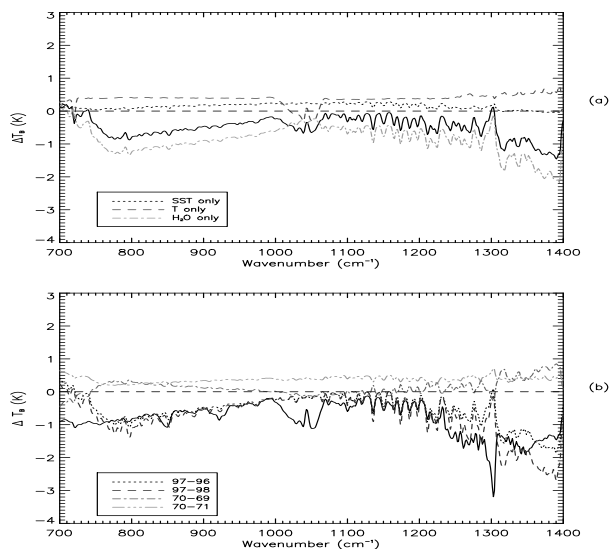


Figure 4. As figure 3 for the West Pacific.

The effects of including long-term changes in the trace gases CO_2 , O_3 , N_2O , CH_4 , CFC11 and CFC12 are shown by the bold curve in figures 3(b) and 4(b). Now the absorption features seen in the observed data are apparent in the simulations, the latter having a comparable magnitude to the former given the measurement uncertainties (fig 1). The lighter curves also shown in figures 3(b) and 4(b) illustrate the mean AMJ

year-year differences in BT over the two extended simulation time periods. Assuming that HADAM3 correctly captures atmospheric variability on monthly time scales, fluctuations in atmospheric temperature and humidity over an individual ENSO event are sufficient to produce BT changes over the window and water vapour vibration-rotation band that are at least of equal magnitude to those seen between AMJ 1997 and 1970. However, the distinctive trace gas signals can only be explained by long-term changes in atmospheric CO_2 , O_3 , CH_4 , CFC11 and CFC12.

5. CONCLUSIONS

By comparing spectrally resolved observations from the IRIS and IMG instruments we have identified clear signatures due to long term changes in trace gas amounts. Although these strongly affect the OLR the atmospheric temperature and humidity response cannot be unequivocally determined owing to the snapshot nature of the observations.

ACKNOWLEDGMENTS

We thank the NASDA for access to the IMG data set, L.Chen and R.Goody for supplying the IRIS data, and R. Allan for providing the HADAM3 fields.

REFERENCES

- Ackerman, S., W. Smith, J. Spinhirne, and H. Revercomb, 1990: The 27-28 October 1986 FIRE IFO cirrus case study: spectral properties of cirrus cloud in the 8-12 μm window. *Mon. Wea. Rev.*, **118**, 2377-2388
- Goody, R., J. Anderson, and G. North, 1998: Testing climate models: an approach. *Bull. Amer. Meteor. Soc.*, **79**, 2541-2549
- Hanel, R.A, B.J. Conrath, V.G. Kunde, C. Prabhakara, I. Revah, V.V. Salomonson, and G. Wolford, 1972: The Nimbus 4 infrared spectroscopy experiment 1. Calibrated thermal emission spectra. *J. Geophys. Res.*, **77**, 2629-2641
- Harries, J.E., H.E. Brindley, P.J. Sagoo, and R.J. Bantges, 2001, Increases in greenhouse forcing inferred from the outgoing longwave radiation spectra of the Earth in 1970 and 1997. *Nature*, **410**, 355-357
- Kobayashi, H., A. Shimota, K. Kondo, E. Okumura, Y. Kameda, H. Shimoda, and T. Ogawa, 1999: Development and evaluation of the interferometric monitor for greenhouse gases: a high-throughput Fourier-transform infrared radiometer for nadir Earth observation. *Appl. Opt.*, **38**, 6801-6807